OPTIMIZING SCHEMES OF FREQUENCY-DEPENDENT AVO INVERSION FOR SEISMIC DISPERSION-BASED HIGH GAS-SATURATION RESERVOIR QUANTITATIVE DELINEATION

XIN LUO[1,2], XUEHUA CHEN[1,2,*], LEIMING SUN[3], JIE ZHANG[2] and WEI JIANG[2]

[1] State Key Laboratory of Oil & Gas Reservoir Geology and Exploitation, Chengdu University of Technology, 1 Erxianqiao Dongsan Road, Chengdu, Sichuan 610059, P.R. China. chen_xuehua@163.com
[2] Key Lab of Earth Exploration and Information Techniques, Chengdu University of Technology, 1 Erxianqiao Dongsan Road, Chengdu, Sichuan 610059, P.R. China. luoxinfd90@163.com, nevr007@yeah.net, stjiangwei23@163.com
[3] Data Processing Company, Geophysical-China Oilfield Services Limited, #788 Nantiao Road, Zhanjiang, Guangdong 524057, P.R. China. sunlm@cosl.com.cn

(Received December 24, 2018; revised version accepted January 30, 2020)

ABSTRACT

Luo, X., Chen, X.H., Sun, L.M., Zhang, J. and Jiang, W., 2020. Optimizing schemes of frequency- dependent AVO inversion for seismic dispersion-based high gas-saturation reservoir quantitative delineation. *Journal of Seismic Exploration*, 29: 173-199.

Previous works demonstrate that dispersion properties can be deduced from frequency-dependent AVO inversion (FDAI). The optimal selection of dispersion-related fluid factors is of great importance to improve the accuracy of fluid identification. In order to quantitatively delineate the reservoir with high gas saturation, we propose an optimal scheme of FDAI to pursue the optimal dispersion factor which is the most sensitive to the high gas saturation reservoir. First, within the seismic frequency band, we construct an objective function to determine the optimal reference frequency by using the dispersion factors calculated from the pre-stack seismic data nearby borehole. Then, we can directly get the optimal dispersion factor related to gas-saturated reservoir according to the fluid indication coefficient. At last, we apply optimal parameters to calculate the dispersion results for seismic data volume. Numerical analysis indicates that the dispersion degree of fluid-saturated reservoir shows an approximate linear increase characteristic with increasing gas saturation. It provides an evidence for the delineation of high gas-saturation reservoirs by using the dispersion anomalies. The seismic field data results illustrate that the dispersion factors inverted by the optimal reference frequency can highlight the dispersion anomalies of gas-saturated reservoirs. Meanwhile, the optimal dispersion factor can delineate the reservoirs with high gas-saturation more accurate while less affected by the background interference of elastic layers than conventional methods. The proposed optimal workflow can improve the accuracy of FDAI and it is feasible to detect the location and spatial distribution of high gas-saturation reservoirs.

KEY WORDS: frequency-dependent AVO inversion, dispersion factor, optimal selection, gas saturation, reservoir delineation.

0963-0651/20/$5.00

INTRODUCTION

Conventional AVO analysis has been proved to be an effective method in hydrocarbon exploration over the past few decades (Smith and Gidlow, 1987; Castagna et al., 1998; Gray, 2002; Russell et al., 2003). It has been commonly observed that the velocity dispersion and attenuation occur when the seismic waves travel through the hydrocarbon saturated porous rocks (Chapman et al., 2003; Batzle et al., 2006; Quintal, 2012; Chen et al., 2013). Here, the attenuation refers to the amplitude decrease, waveform distortion and the phenomenon of dominant frequency shifts to lower frequency when seismic wave propagates through a fluid-saturated medium. Dispersion is the variation of seismic wave velocity with frequency during seismic wave propagation. However, the conventional AVO analysis does not take the dispersion features of seismic wave propagation into consideration and ignores the frequency-dependent effects. Intensive studies suggest that velocity dispersion and attenuation provide frequency-dependent anomalies associated with hydrocarbon-bearing rocks (Brown, 2009; Chapman et al., 2009). When fluids are contained in the pore space of rocks, the mechanism that causes frequency-dependent dispersion and attenuation is known as wave-induced fluid flow (WIFF) (Biot, 1962; Mavko and Nur, 1975; White, 1975; Brown, 2009; Müller et al., 2010; Rubino et al., 2012) which results in frequency-dependent AVO response. That is, the seismic reflection coefficients are not only related to the incidence angle, but also vary with frequencies (Chapman et al., 2005; Silin et al., 2006; Silin and Goloshbin, 2010).

Many studies show that dispersion and attenuation caused by the fluid flow may occur in the seismic frequency range (Batzle et al., 2001; Korneev et al., 2004; Chapman et al. 2006, 2009; Gurevich et al., 2010; de Paula et al., 2012). For years, geophysicists preferred to explain the mechanism of velocity dispersion and attenuation by different theoretical equivalent models. For instance, the local fluid-flow or squirt-flow model (Dvorkin et al., 1995; Gurevich et al., 2010) and the dual-porosity model (Pride and Berryman, 2003a, 2003b). White (1975) proposed the patchy-saturation model to study the mesoscopic mechanism and explained the velocity dispersion and attenuation in the seismic spectral band. This model was then extended and modified by other researchers (Dutta et al., 1979; Johnson, 2001). For the anisotropic case, Chapman et al. (2002, 2003) proposed a multi-scale equant porosity model to numerically model the velocity dispersion and attenuation of fluid-saturated rocks. All the studies illustrate that fluid-saturated reservoirs lead to frequency-dependent dispersion and attenuation which are preferable to hydrocarbon detection.

Thus, understanding the mechanism of fluid-related dispersion is of great importance to pursue hydrocarbon indicators for fluid identification in reservoir delineation. The numerical modeling for velocity dispersion and attenuation and frequency-dependent AVO analyses have been studied by researchers (Rubino et al., 2009; Liu et al., 2011; Chen et al., 2016, 2017). Xu et al. (2011) used the frequency-dependent seismic reflection coefficient

for discriminating gas reservoirs. Chen et al. (2012, 2013) proposed fluid mobility attribute for gas reservoir delineation based on the frequency-dependent response. Ghosal et al. (2018) performed the dispersion analysis of velocity and reflectivity. Meanwhile, estimation of attenuation attributes is of great importance for exploring the attenuation characteristics of fluid-saturated reservoirs (Bradford, 2007; Quintal, 2012; Beckwith et al., 2017). It is also a key factor for seismic processing and migration images (Yang et al., 2018).

To extract the dispersion anomalies induced by fluid flow from pre-stack field data, Wilson et al. (2009) and Wu et al. (2010, 2012) proposed a frequency-dependent AVO inversion (FDAI) method. Recently, considerable attention has been paid to predict hydrocarbon reservoirs and gas saturation by using the dispersion-related fluid factors obtained from FDAI (Wu et al., 2012, 2014; Cheng et al. 2012; Chen et al., 2012, 2014; Zhang et al., 2011; Zong et al., 2016; Zhong et al., 2017). However, the FDAI method is routinely based on the AVO linear approximation proposed by Smith and Gidlow (1987) to invert the dispersion factors which are obtained from the frequency-dependent velocities of the P- and S-wave. Zhang et al. (2014) proposed a new dispersion factor which is deduced from the frequency-dependent fluid term based on f-μ-ρ AVO approximation (Russell et al., 2003). All these dispersion factors are beneficial to identify the dispersion phenomena caused by fluid-saturated media while not necessarily sensitive for the delineation of high gas saturation reservoirs.

In our work, the study area is sandstone reservoir saturated with different gas saturation. To explore the high gas saturation (Sg > 40%) reservoir is of great significance for marine exploration. In order to pursue the optimal dispersion factor to quantitatively delineate the reservoir with high gas-saturation and improve the reliability of hydrocarbon detection, we propose an optimal workflow of FDAI to pursue the optimal dispersion factor. First, we quantitatively analyze the velocity dispersion and attenuation and the frequency-dependent AVO response of reservoirs saturated with different gas saturations based on the real log data. Then, to obtain the most sensitive dispersion factor related to high gas-saturation reservoirs, we review the FDAI method and construct an objective function to select the optimal reference frequency. This can maximize the dispersion anomalies of hydrocarbon reservoirs and make the dispersion differences of different fluids reach the maximum. Next, we define a fluid indication coefficient for selecting the optimal dispersion factor. This enables us to suppress the interference of elastic layers and to produce high-accuracy dispersion results only related to high gas-saturation reservoirs. Finally, we use field data examples to illustrate the effectiveness of our optimizing schemes.

THEORY AND METHOD

Frequency-dependent AVO inversion

Wilson et al. (2009) and Wu et al. (2010, 2012) extended the two-term AVO linear approximation proposed by Smith and Gidlow (1987) to frequency domain and obtained the dispersion factors I_a and I_b which are deduced from the derivatives of frequency-dependent velocities of P- and S-wave. Their expressions are written as

$$I_a = \frac{d}{d\omega}\left(\frac{\Delta v_p}{v_p}\right),\ I_b = \frac{d}{d\omega}\left(\frac{\Delta v_s}{v_s}\right) \tag{1}$$

Zhang et al. (2014) introduced a dispersion factor I_f which is deduced from frequency-dependent fluid term based on the *f*-μ-ρ AVO approximation proposed by Russell et al. (2011).

$$R(\theta) = \left[(\frac{1}{4} - \frac{\gamma^2{}_{dry}}{4\gamma^2{}_{sat}})\frac{\sec^2\theta}{4}\right]\frac{\Delta f}{f} + \left[\frac{\gamma^2{}_{dry}}{4\gamma^2{}_{sat}}\sec^2\theta - \frac{2}{\gamma^2{}_{sat}}\sin^2\theta\right]\frac{\Delta\mu}{\mu} + \left[\frac{1}{2} - \frac{\sec^2\theta}{4}\right]\frac{\Delta\rho}{\rho}\ , \tag{2}$$

where $R(\theta)$ is derived from the theory of poroelasticity and is the P-wave reflection coefficient (a ratio of the amplitudes of incident and reflected waves) for an incident plane wave across an interface between two elastic media, and it mainly represent the difference of elastic parameters at the interface of two elastic media for different incident angles. f, μ and ρ are the fluid term, shear modulus and density, respectively. The expression form of γ^2_{sat} and γ^2_{dry} can be expressed as:

$$\gamma^2_{sat} = \left(\frac{V_p}{V_s}\right)^2_{sat},\ \gamma^2_{dry} = \left(\frac{V_p}{V_s}\right)^2_{dry}\ . \tag{3}$$

Russell et al. (2011) discussed the different forms of eq. (2) at different values of γ^2_{dry}. Here, we set $r = \gamma^2_{dry}$. If we let r = 2 and r = 4/3, eq. (2) reduces to the λ-μ-ρ and K-μ-ρ AVO approximation, respectively. As discussed by Russell et al. (2003), the r values are not appropriate for typical saturated rocks and the measurement from real lithology illustrated that r values as high as 3 for sandstone reservoirs. In our work, we only discuss the r values within the range of 4/3 to 3 since the target reservoirs are sandstone in our field data example.

The fluid term f and shear modulus μ can be expressed as:

$$f = \rho V_P^2 - \rho\gamma^2_{dry}V_S^2, \mu = \rho V_S^2\ . \tag{4}$$

Then, $\Delta f/f$ and $\Delta\mu/\mu$ can be written as:

$$\frac{\Delta f}{f}=\left(\frac{\partial f}{\partial V_P}\Delta V_P+\frac{\partial f}{\partial \rho}\Delta\rho\right)\Bigg/\left[\left(1-\frac{\gamma_{dry}^2}{\gamma_{sat}^2}\right)\rho V_p^2\right]=2\frac{\Delta V_P}{V_P}+\frac{\Delta\rho}{\rho} \quad , \tag{5}$$

and

$$\frac{\Delta\mu}{\mu}=\left(\frac{\partial \mu}{\partial V_s}\Delta V_s+\frac{\partial \mu}{\partial \rho}\Delta\rho\right)\Big/\left(\rho V_s^{\,2}\right)=2\frac{\Delta V_S}{V_S}+\frac{\Delta\rho}{\rho} \quad . \tag{6}$$

Note that $\Delta f/f$ and $\Delta\mu/\mu$ are related to the velocity of V_p and V_s according to the eqs. (5) and (6). Thus, $\Delta f/f$ and $\Delta\mu/\mu$ are also frequency-dependent due to the frequency-dependent velocities. Here, we suppose the relative change of property $\Delta\rho/\rho$ is sufficiently small that can be neglected. Then, eq. (2) can be extended to the frequency domain.

$$R\left(\theta_i,\omega_j\right)\approx A\left(\theta_i\right)\frac{\Delta f}{f}\left(\omega_j\right)+B\left(\theta_i\right)\frac{\Delta\mu}{\mu}\left(\omega_j\right) \quad , \tag{7}$$

where ω is the angular frequency, and $A(\theta)$ and $B(\theta)$ are defined as:

$$A\left(\theta_i\right)=\left(\frac{1}{4}-\frac{\gamma^2{}_{dry}}{4\gamma^2{}_{sat}}\right)\frac{\sec^2\theta}{4} \quad , \tag{8}$$

and

$$B\left(\theta_i\right)=\frac{\gamma^2{}_{dry}}{4\gamma^2{}_{sat}}\sec^2\theta-\frac{2}{\gamma^2{}_{sat}}\sin^2\theta \quad . \tag{9}$$

Eq. (7) can be expanded as first-order Taylor series at a reference frequency f_0 ($f_0=\omega_0/2\pi$) without considering the higher-order terms.

$$R\left(\theta_i,\omega_i\right)\approx A\left(\theta_i\right)\frac{\Delta f}{f}\left(\omega_0\right)+\left(\omega_j-\omega_0\right)A\left(\theta_i\right)I_f+B\left(\theta_i\right)\frac{\Delta\mu}{\mu}\left(\omega_0\right)+\left(\omega_j-\omega_0\right)B\left(\theta_i\right)I_\mu \quad . \tag{10}$$

Here, we define I_f and I_μ as the dispersion factor of fluid term and shear modulus respectively, and they are expressed as:

$$I_f=\frac{d}{d\omega}\left(\frac{\Delta f}{f}\right),\ I_\mu=\frac{d}{d\omega}\left(\frac{\Delta\mu}{\mu}\right) \quad . \tag{11}$$

Then eq. (10) can be written as:

$$R\left(\theta_i,\omega_j\right)-A\left(\theta_i\right)\frac{\Delta f}{f}\left(\omega_0\right)-B\left(\theta_i\right)\frac{\Delta\mu}{\mu}\left(\omega_0\right)\approx\left[\left(\omega_j-\omega_0\right)A\left(\theta_i\right)\quad\left(\omega_j-\omega_0\right)B\left(\theta_i\right)\right]\begin{bmatrix}I_f\\I_\mu\end{bmatrix} \tag{12}$$

We assume that we know the velocity model so that the coefficients $A(\theta_i)$ and $B(\theta_i)$ can be calculated through ray tracing method and they can make the replacement by $A(t,n)$ and $B(t,n)$, respectively. Therefore, considering m frequencies [ω_1, ω_2,…, ω_m], the vectors **r** and **e** can be expressed in matrix form:

$$\mathbf{r}=\begin{bmatrix} R(t,1,\omega_1)-A(t,1)\frac{\Delta f}{f}(t,\omega_0)-B(t,1)\frac{\Delta\mu}{\mu}(t,\omega_0) \\ \vdots \\ R(t,1,\omega_m)-A(t,1)\frac{\Delta f}{f}(t,\omega_0)-B(t,1)\frac{\Delta\mu}{\mu}(t,\omega_0) \\ \vdots \\ R(t,n,\omega_1)-A(t,n)\frac{\Delta f}{f}(t,\omega_0)-B(t,n)\frac{\Delta\mu}{\mu}(t,\omega_0) \\ \vdots \\ R(t,n,\omega_m)-A(t,n)\frac{\Delta f}{f}(t,\omega_0)-B(t,n)\frac{\Delta\mu}{\mu}(t,\omega_0) \end{bmatrix} \tag{13}$$

and

$$\mathbf{e}=\begin{bmatrix} (\omega_1-\omega_0)A(t,1) & (\omega_1-\omega_0)B(t,1) \\ \vdots & \vdots \\ (\omega_m-\omega_0)A(t,1) & (\omega_m-\omega_0)B(t,1) \\ \vdots & \vdots \\ (\omega_1-\omega_0)A(t,n) & (\omega_1-\omega_0)B(t,n) \\ \vdots & \vdots \\ (\omega_m-\omega_0)A(t,n) & (\omega_m-\omega_0)B(t,n) \end{bmatrix} . \tag{14}$$

Then, we can obtain:

$$\mathbf{r}\approx\mathbf{e}\begin{bmatrix} I_f \\ I_\mu \end{bmatrix} . \tag{15}$$

At last, the least-squares inversion method can be used to estimate the frequency-dependent attributes I_f and I_μ:

$$\begin{bmatrix} I_f \\ I_\mu \end{bmatrix}\approx\left(\mathbf{e}^{\mathrm{T}}\mathbf{e}\right)^{-1}\mathbf{e}^{\mathrm{T}}\mathbf{r} . \tag{16}$$

The FDAVO inversion method is to extract the dispersion information from the amplitudes of reflection coefficients. However, the seismic amplitudes contain overprint of the source wavelet, so it must be removed if

the true spectral behavior of the fluid-saturated reservoir is obtained. Thus, this method strongly relies on a spectral decomposition and balancing process to remove this wavelet effect. Here, spectral decomposition is based on generalized S-transform (GST) (Chen et al., 2008).

$$S(f,\tau)=\int_{-\infty}^{+\infty}x(t)\frac{|\beta||f|^{p}}{\sqrt{2\pi}}\exp\left[-\frac{\beta^{2}(t-\tau)^{2}f^{2p}}{2}\right]\exp(-i2\pi f)dt \quad , \qquad (17)$$

where, β, p are the regulatory factors, $x(t)$ is the original signal and f is the frequency.

For a partial stack with n traces denoted as a data matrix $s(t, n)$, we perform GST on $s(t, n)$ to obtain time-frequency spectra $S(t, n, f)$. The wavelet overprint contained in S is removed through spectral balancing by the following weight function w:

$$w(f_i,n)=\frac{\max\left[S_{f_0}(n)\right]}{\max\left[S_{f_i}(n)\right]} \quad , \qquad (18)$$

where, $\max[S_{f_0}(n)]$ and $\max[S_{f_i}(n)]$ refer to the maximum amplitude of the n^{th} trace at reference frequency f_0 and each individual frequency f_i, respectively. Then, we use the weight function $w(f_i,n)$ to balance the amplitudes of all spectral components of seismic traces by the equation:

$$S_{f_i}^{b}(t,n)=S_{f_i}(t,n)w(f_i,n) \quad . \qquad (19)$$

The scheme for determining the optimal reference frequency

The selection of reference frequency is significant for FDAI since an appropriate reference frequency can directly influence the accuracy of inversion result associated with the gas saturation. In general, the selection of reference frequency is determined by empirical observations from spectral decomposition and the dominant frequency of the seismic signal is usually selected as the reference frequency (Wilson et al., 2009; Wu et al., 2010, 2012). However, the method cannot accurately determine the most sensitive reference frequency which can maximize the dispersion anomalies of hydrocarbon reservoirs and makes the dispersion difference of different fluids reach the maximize value. Thus, we propose an optimal workflow to determine the optimal reference frequency f_{opt}. The main steps are as follows:

1) Within seismic frequency band, using all frequency components of the seismic data nearby bore-hole as reference frequency to calculate the dispersion factors based on FDAI at the target intervals.
2) According to the result of log interpretation, dispersion factors of all

reference frequencies calculated are used to construct an objective function $D(t,f)$ which is the 2D dispersion distribution in frequency and time domain

$$D(t,f)=\left[I_s(t,f_1);I_s(t,f_2);I_s(t,f_3);...;I_s(t,f_m)\right] \quad , \tag{20}$$

where $[f_1,f_2,f_3,\ldots,f_m]$ are reference frequencies within the seismic frequency band, I_s ($s = a,b,f,\mu$) is the dispersion factor calculated from different elastic modulus.

3) Then, extracting dispersion curves at specific time locations (the top and bottom of high gas saturation reservoirs) and use the cross-plot analysis to pick up the optimal reference frequency f_{opt} when dispersion factors obtain their maximum value

$$f_{opt}=\max_{f}\left[D_t,D_b\right] \quad , \tag{21}$$

where D_t and D_b are the dispersion curves extracted from the objective function $D(t,f)$ at the time location of top and bottom of high gas saturation reservoirs, respectively.

4) Using the f_{opt} of step (3) selected as the optimal reference frequency in FDAI to process the pre-stack angle gathers of whole area. Dispersion factors obtained in this case can maximize the dispersion anomalies of gas-saturated reservoirs.

The scheme for determining the optimal dispersion factor

The optimal dispersion factor should be further selected due to the sensitivity difference in FDAI-based gas saturation delineation. According to the equation (10), we can obtain different dispersion factors when the parameter r changes. How to select the optimal dispersion factor is the key to improve the accuracy of fluid identification by using the dispersion anomalies. Thus, we propose a workflow for selecting the optimal dispersion factor.

Here, we use the optimal reference frequency f_{opt} to calculate the dispersion factors, and the optimal dispersion factor is selected when the r values within the range of 4/3 to 3. The main steps of the method are as follows:

1) To obtain the dispersion factors of the seismic data nearby bole-hole when r given different values.

2) The dispersion factor I_f obtained and the parameter r are used to construct the objective function $F(t,r_i)$:

$$F\left(t,r_i\right)=\frac{\partial}{\partial\omega}\left(\frac{\Delta f}{f}\right)\Bigg|_{r_i} \quad . \tag{22}$$

3) According to the result of log interpretation. We regard fluid-saturated interval as the interpreted layers and the layers outside the interpreted layers are elastic. Extract the dispersion curves at the time location of the fluid-saturated and elastic layers from the objective function $F(t,r_i)$ to analyze.
4) Calculate the fluid indication coefficient $c(r_i)$ using the equation (23) and to determine the optimal parameter r_{opt} when $c(r_i)$ gets the maximum value.

$$c\left(r_i\right)=\frac{F\left(t_f,r_i\right)-F\left(t_e,r_i\right)}{F\left(t_e,r_i\right)} \quad , \tag{23}$$

where c is the fluid indication coefficient, t_f and t_e are the time points at fluid-saturated stratum and elastic layer, respectively.

According to the above steps, we can get the optimal dispersion factor related to fluids when c(r_i) gets the maximum. The optimal parameter r_{opt} selected as follows:

$$r_{opt}=\max_{r_i}\left[c\left(r_i\right)\right] \quad . \tag{24}$$

NUMERICAL ANALYSIS

In order to quantitatively delineate the reservoir with high gas saturation, we analyzed the frequency-dependent velocities and attenuations of fluid-saturated reservoirs with different gas saturation based on the real log curves. Fig. 1 shows the well-logs through the sandstone reservoir, including water saturation (Sw), P-wave, S-wave and density curves. The color rectangles outlines the fluid-saturated reservoirs saturated with different gas saturation (high gas-saturated zone with the S_g= 0.6, low gas-saturated zone with the S_g= 0.3 and water-saturated zone with the S_g= 0). The S-wave curve in the third column shows high values. However, the P-wave velocity (in the second column) and density curves (in the fourth column) show a change to lower values, corresponding to the elastic zone. According to the analysis of log curves, the elastic parameters (P-wave, S-wave and density) are difficult for identifying the reservoir with high gas saturation.

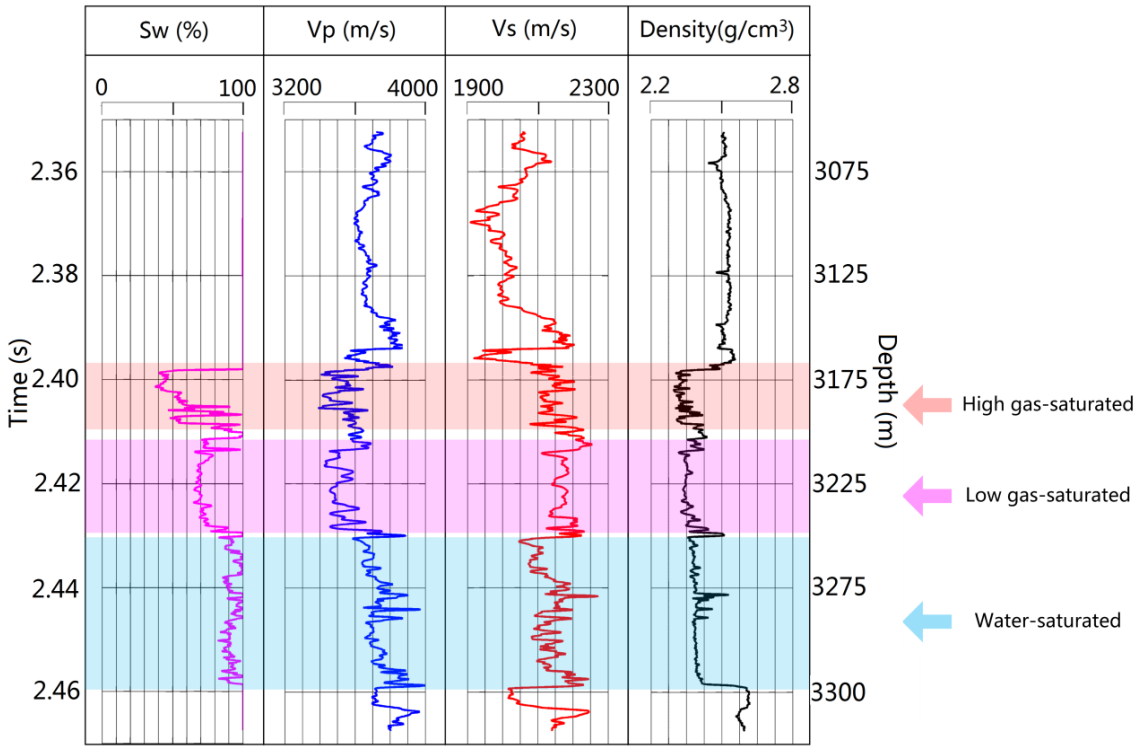

Fig. 1. Well log curves of the sandstone reservoir.

Then, we follow the work of Chapman et al. (2003) to calculate the frequency-dependent velocities and attenuations (the theoretical background is exhibited in Appendix A) of the hydrocarbon reservoirs saturated with different gas saturations (outlined by three different color rectangles in Fig.1). The parameters (Table 1) of fluid-saturated reservoirs used in the calculations are given by the real log data. The porosity of porous medium is 18% given from the real log data and other parameters are given as follows: crack density is 0.1, crack radius is 2.75 mm and aspect ratio is 0.0036. The basic properties of gas and water used in numerical modeling are calculated by the equations of Batzle and Wang (1992) at a pressure of 25 Mpa, a temperature of 50 ℃, a salinity of 100,000 PPM, a density of dead oil of 0.75 g/cm^3 and a gas to air density ratio set at 0.65.The physical parameters of gas and water are given in Table 2.

Table 1. The parameters of fluid-saturated reservoirs used in the calculations.

Properties	High gas-saturated	Low gas-saturated	Water-saturated
Vp (m/s)	3465	3500	3700
Vs (m/s)	2147	2165	2135
Sg (%)	0.6	0.3	0

Table 2: Fluid properties used in the calculations.

Properties	Gas	Water
Density (g/cm^3)	201.6	1068.2
Bulk modulus (MPa)	60.6122	3024.4
Dynamic viscosity (cP)	0.0254	0.755

Fig. 2 shows the frequency-dependent velocities and attenuation and there are differences in velocity dispersion and attenuation at different gas saturations. The velocity moves toward higher value with decreasing gas saturation. Note that the attenuation peaks of $1/Q_p$ and $1/Q_s$ shown in Figs.2c-2d get the maximum values when $S_g = 0$ and get the minimum values when $S_g = 0.6$, whereas the attenuation peaks for $S_g = 0.3$ intermediated between $S_g = 0.6$ and $S_g = 0$. Both attenuation peaks for $1/Q_p$ and $1/Q_s$ decrease with increasing gas saturations. However, the characteristic frequency at which the peak attenuation occur shifts to a higher frequency as the gas saturation increases from 0 to 0.6. Thus, the information of velocity dispersion and attenuation are beneficial for our work to delineate the high gas saturation reservoir. Meanwhile, the P-wave velocity shows a larger difference between high and low frequency relative to the S-wave. Figs.2c-2d shows the attenuation value of S-wave is small compared to the P-wave case due to the shear modulus is decoupled from the saturating fluid. This phenomenon indicates that the velocity dispersion of a P-wave is more obvious than for an S-wave.

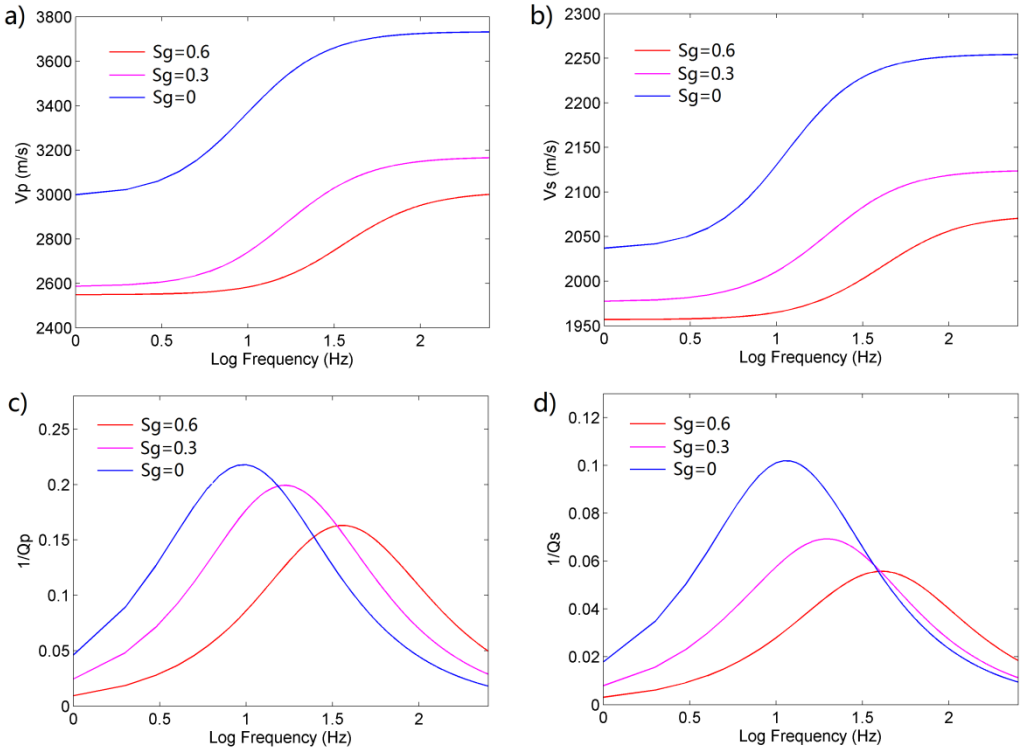

Fig. 2. Frequency-dependent velocities of (a) P-wave and (b) S-wave and the inverse quality factors (c) $1/Q_p$ and (d) $1/Q_s$ at gas saturations of 0.6, 0.3, and 0, respectively.

Due to the characteristics of frequency-dependent velocities, the reflection coefficients at the top and bottom of the reservoirs will also show frequency-dependent characteristics. According to the three-term AVO linear approximation formula proposed by Wiggins et al. (1983), we can calculate the frequency-dependent reflection coefficients versus incident angles by using the frequency-dependent velocities. Here, we only analyze the reflection coefficients at the top and bottom interfaces of the high gas-saturation reservoir. The results are shown in Fig. 3. Note that the reflection coefficients are frequency-dependent at different incidence angles and the absolute value of the reflection coefficients at top and bottom interfaces decrease with increasing frequencies.

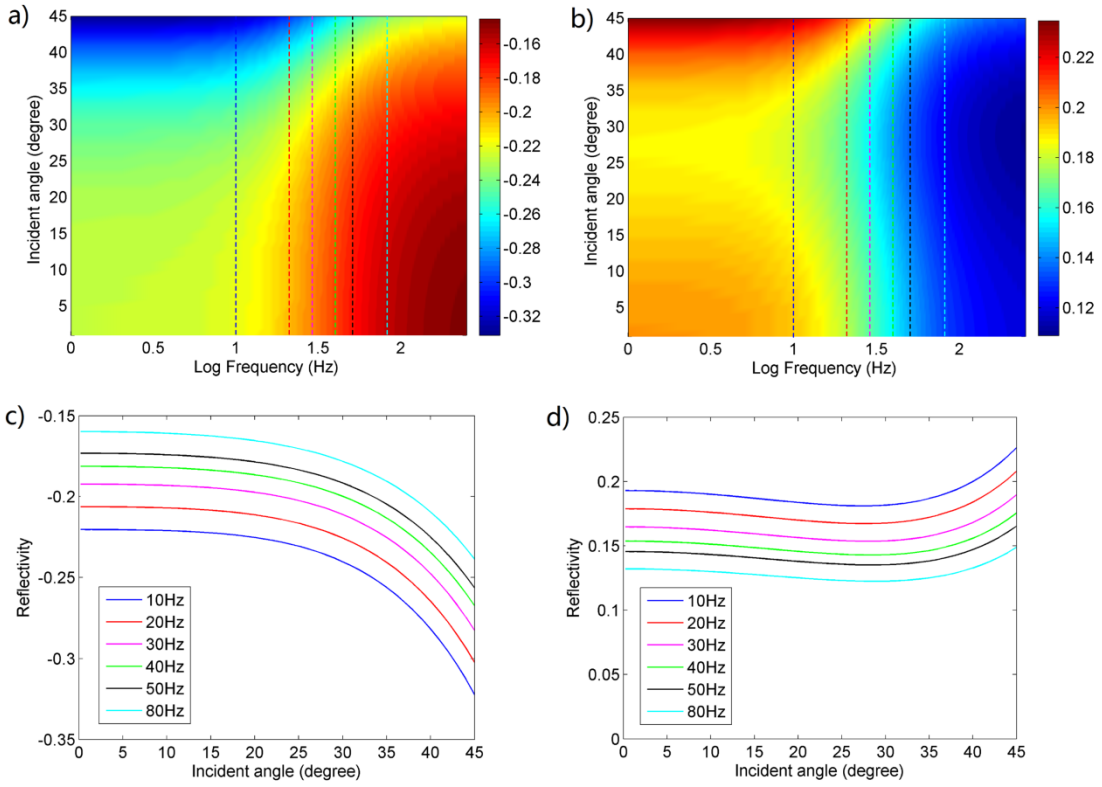

Fig. 3. Frequency-dependent reflection coefficients distributions at (a) top interface and (b) bottom interface, and the corresponding reflection coefficients of (c) top interface and (d) bottom interface at 6 specific frequencies. The dashed lines marked in (a) and (b) denote the corresponding location at 6 specific frequencies of 10 Hz, 20 Hz, 30 Hz, 40 Hz, 50 Hz, and 80 Hz.

Our research focuses on the frequency-dependent behaviors of the high gas saturation reservoir saturated with different gas saturation. In order to better quantitatively delineate the reservoir with high gas-saturation, we calculate the velocity dispersion and attenuation when the gas saturation varies from 0 to 1. Fig. 4a shows the frequency-dependent velocities of the P-wave in the case of a gas-water saturated reservoir when the gas saturation within the range of 0 to 1. Fig. 4b shows that the attenuation peak varies non-linearly with increasing gas saturations in the frequency-saturation plane.

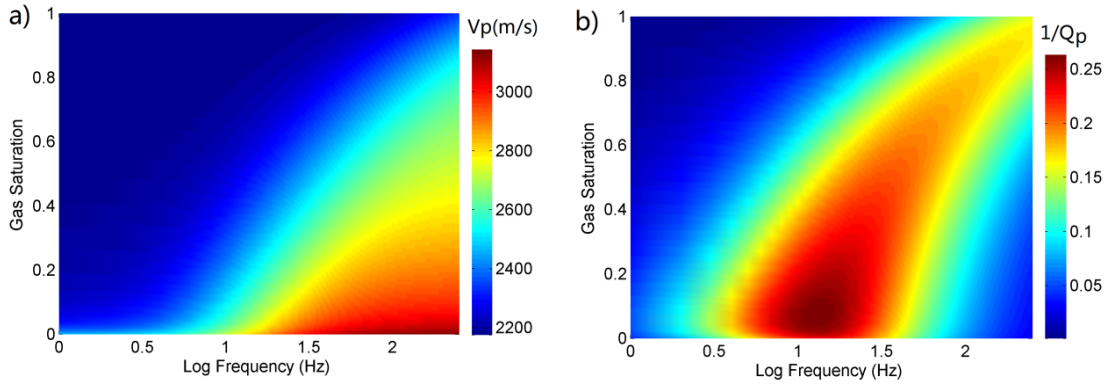

Fig. 4. Frequency-dependent (a) velocities and (b) attenuation of P-wave as functions of both frequency and gas saturation.

Next, we perform a 1D simulation of seismic wave propagation using the phase-shift wavefield extrapolation method in the frequency wavenumber domain (Appendix B) to obtain the seismic responses for the case of gas saturation changes from 0 to1. The synthetic seismic records shown in Fig. 5 were generated by using a Ricker wavelet with the dominant frequency of 35Hz. As shown in Fig. 5, the time range of the seismic gather is only about 0.12 s due to the imited length of logging data. The seismic reflection at the bottom interface of the saturated sandstone reservoir shown in Fig. 5 indicates that the travel time delay increases nonlinearly with increasing gas saturation. The energy of the top reflection enhances with increasing gas saturation, whereas there is energy loss clearly at the bottom reflection for higher gas saturation. The main cause of this phenomenon is that the energy is absorbed more seriously when the seismic wave passes through the higher gas saturation reservoir, which results in the stronger velocity dispersion and attenuation.

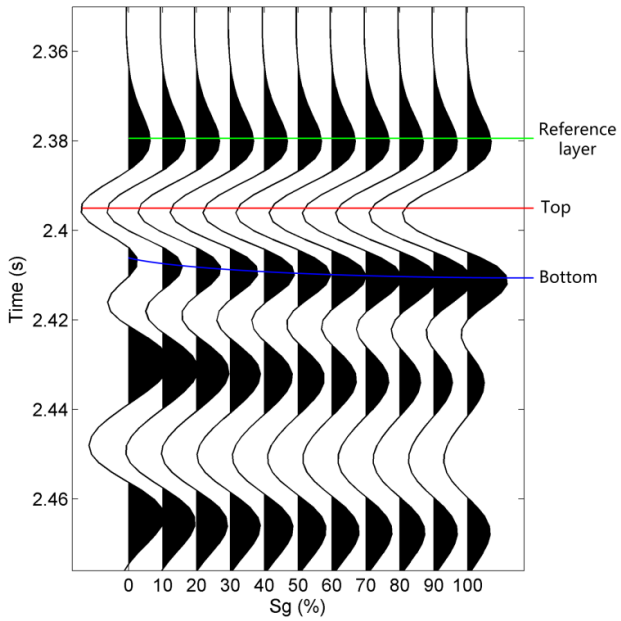

Fig. 5. 1D seismic responses of the sandstone reservoir for the cases of gas saturation changing from 0 to1.

We calculate dispersion factors to analyze the dispersion characteristics when gas saturation changes based on the seismic gather shown in Fig. 5. In the calculation, the choice of reference elastic layer is of critical importance to spectral balancing operation that can affects the accuracy of dispersion results. In dispersion inversion on the synthetic seismic gather, we choose the layer at the waveform trough position above immediately the top interface as the reference layer (indicated by a green line in Fig. 5) to calculate dispersion factors. According to the numerical modeling results in Fig. 2, the S-wave dispersion is significantly smaller than those of the P-wave. The reason is that the shear modulus is decoupled from the saturating fluids. Theoretically, the shear modulus can be expressed as $\mu=\rho v_s^2$ and the density is frequency-independent, so the two dispersion characteristics of S-wave and shear modulus are consistent except for the order. Therefore, we only calculate the dispersion factor I_a [eq. (1)] and I_f [eq. (11)] to analyze. Here, the dispersion factor I_f is obtained when r = 2. Fig. 6 show the results of quantitative analysis of I_a and I_f. As shown in Fig. 6, the dispersion degree of I_a and I_f show a linear increase trend approximately with increasing gas saturation. However, the slopes of dispersion curves are greater when S_g is between 0 and 0.1. These phenomena are beneficial to quantitatively delineate the reservoirs with high gas saturation.

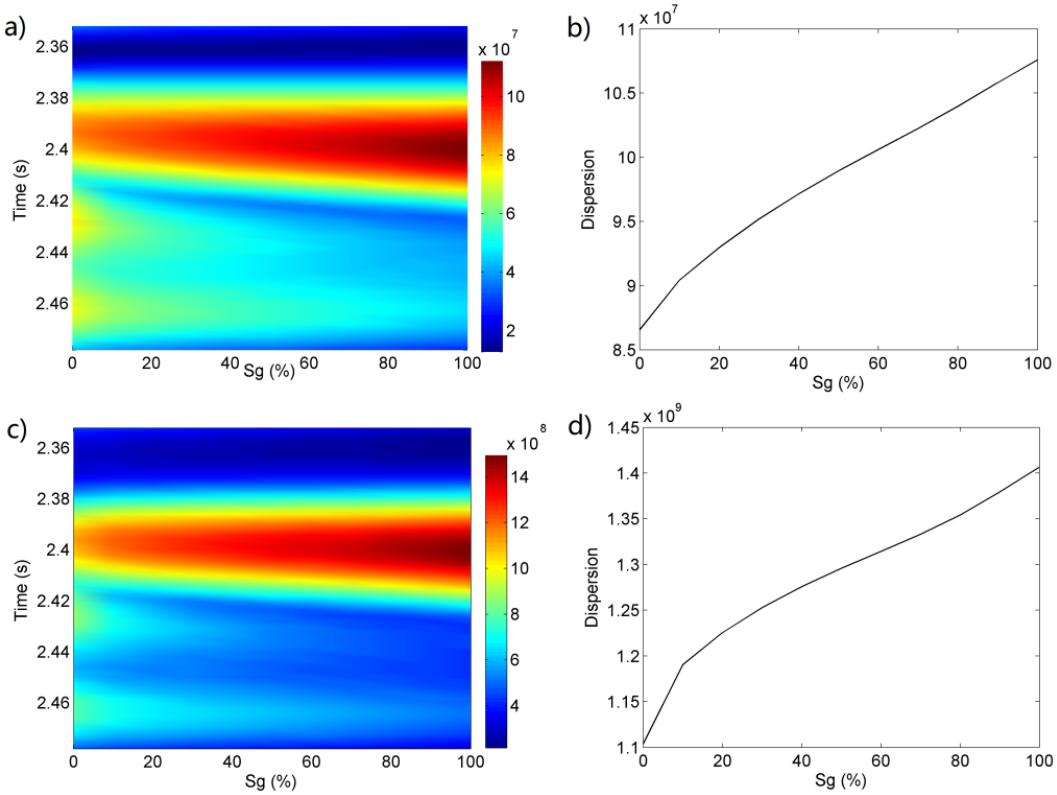

Fig. 6. (a) The 2D distribution of I_a when gas saturation varies from 0 to 1 and (b) its dispersion curve extracted from the reservoir interval; (c) The 2D distribution of I_f when gas saturation varies from 0 to1 and (d) its dispersion curve extracted from the reservoir interval.

FIELD DATA EXAMPLE

The methodology and workflow described above are now applied to field seismic data to evaluate the performance of our method. Fig. 7 shows the stacked profile. The reservoir in the study area is gas-saturated sandstone and the high gas saturation zone is located in the position indicated by a yellow arrow. Fig. 8a shows the angle gathers at the location of a drilled well. Figs. 8b and 8c are the stacked trace of the pre-stack angle traces and its time-frequency spectrum, respectively. In Fig. 8c, there are strong energy clusters at the interpreted layers between the red lines.

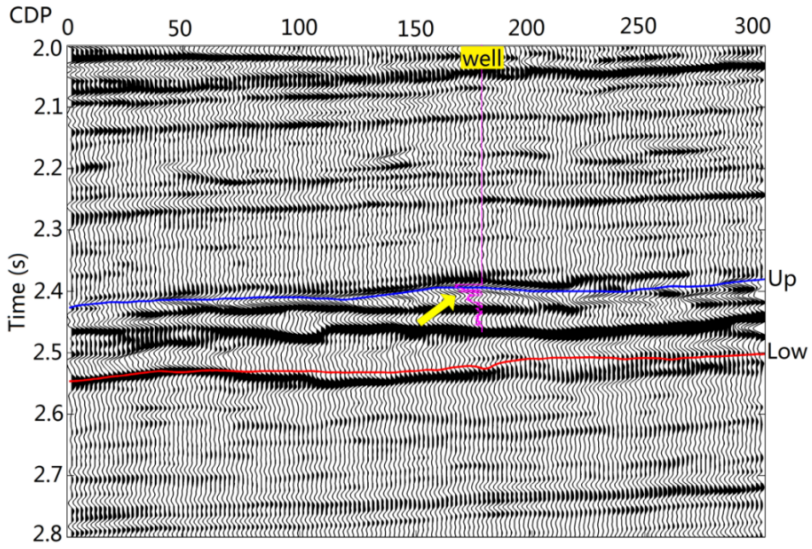

Fig. 7. Stacked seismic profile.

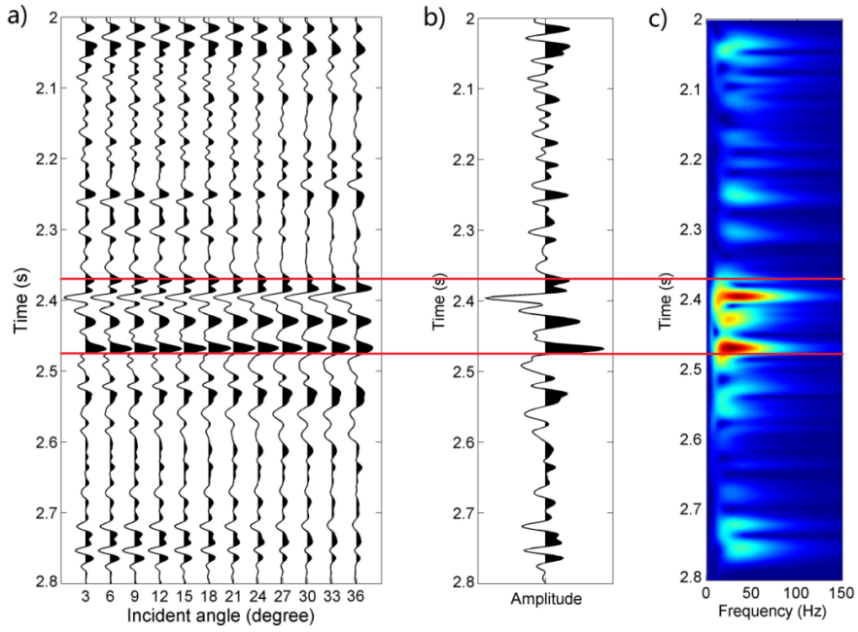

Fig. 8. (a) Seismic angle gathers at the location of the well; (b) Stacked trace of the angle gathers and (c) its time-frequency spectrum.

Optimal selection of reference frequency

For an effective application of the FDAI method to the real field data, we optimize the reference frequency f_{opt} and parameter r using our proposed method. First, we use dispersion factors I_a and I_f in the target interpreted layers to pursue the optimal reference frequency f_{opt}. Here, the dispersion factor I_f is obtained when r = 2. Figs. 9c and 9d illustrate that the optimal reference frequency is about 24 Hz when dispersion value gets the maximum value. The dispersion anomalies approach to peaks when the dispersion factors are calculated by the FDAI in this case, which also makes that the dispersion contrasts of different fluids reach the maxima. Meanwhile, we observe that the P-wave dispersion of the high gas saturation zone is greatly affected by the dispersion anomalies of water-saturated zone (green arrow indicates) in Fig. 9a, whereas the dispersion factor I_f obtained when r = 2 show significant dispersion anomalies in high gas saturation zone and degrade the anomalies of water-saturated zone in Fig. 9b.

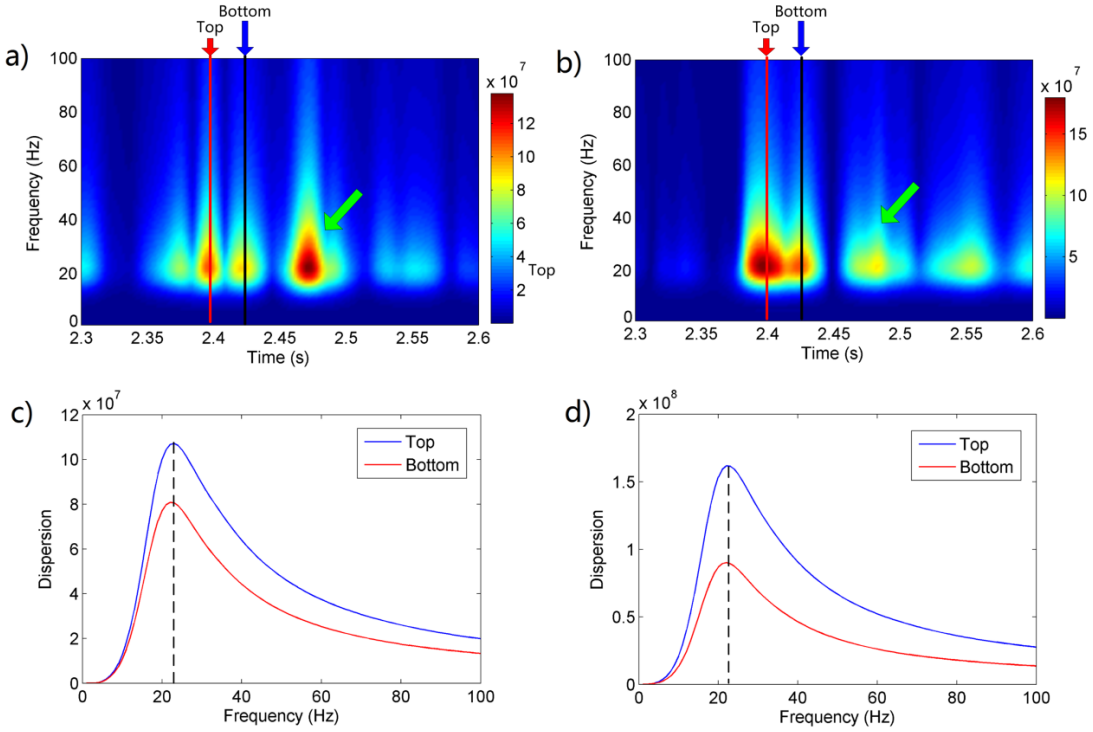

Fig. 9. The dispersion distribution of (a) I_a and (b) I_f in frequency and time domain, and the dispersion curves (c) extracted from (a) and (d) from (b), respectively. Here, the top and bottom indicate the interfaces of high gas saturation reservoir.

Optimal selection of the parameter *r*

As shown in Fig. 10a, the background interference of elastic layers show weak value in the rectangle zones. To further pursue the optimal parameter r, we choose the dispersion curves at the time point of fluid-saturated location and elastic interface for analysis. Fig. 10b indicates that the dispersion

anomalies of fluid-saturated interfaces are all prominent, whereas they decrease with increasing r. However, the background interference of the elastic layer decreases first and then increases with the changing r, and gets the minimum value when r is nearly equal to 2. In order to obtain the dispersion factor which is sensitive to fluid while less affected by the background interference, we calculate the fluid indication coefficient and the results shown in Fig. 10c and 10d.

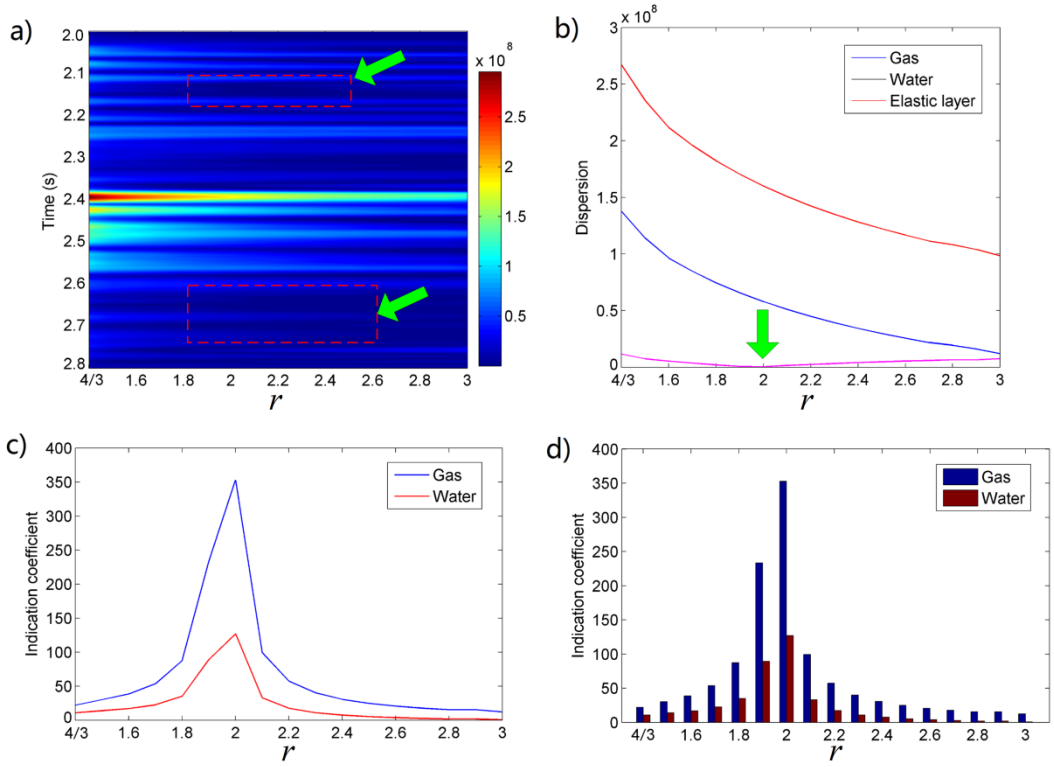

Fig. 10. (a) The 2D (r & Time) distribution of I_f and (b) the dispersion curves at specific interfaces; (c) The fluid indication coefficients of fluid-saturated interfaces and (d) its distribution as a column map.

Figs. 10c and 10d illustrate that the indication coefficients of fluid-saturated zone reaches the maximum value when r = 2 and the dispersion factor obtained in this case is the most sensitive to gas reservoir. Therefore, when we select r = 2 as the optimal parameter for FDAI, the dispersion factor obtained in this case is the most sensitive to high gas-saturation reservoir and less affected by the background interference of other layers.

The results analysis

Finally, we calculate the dispersion factor by FDAI method after choosing the optimal parameters f_{opt} and r. To illustrate the accuracy of the method, we choose three dispersion factor curves near the bore-hole to compare with the result obtained by our method. Fig. 11 shows the results of comparative analysis.

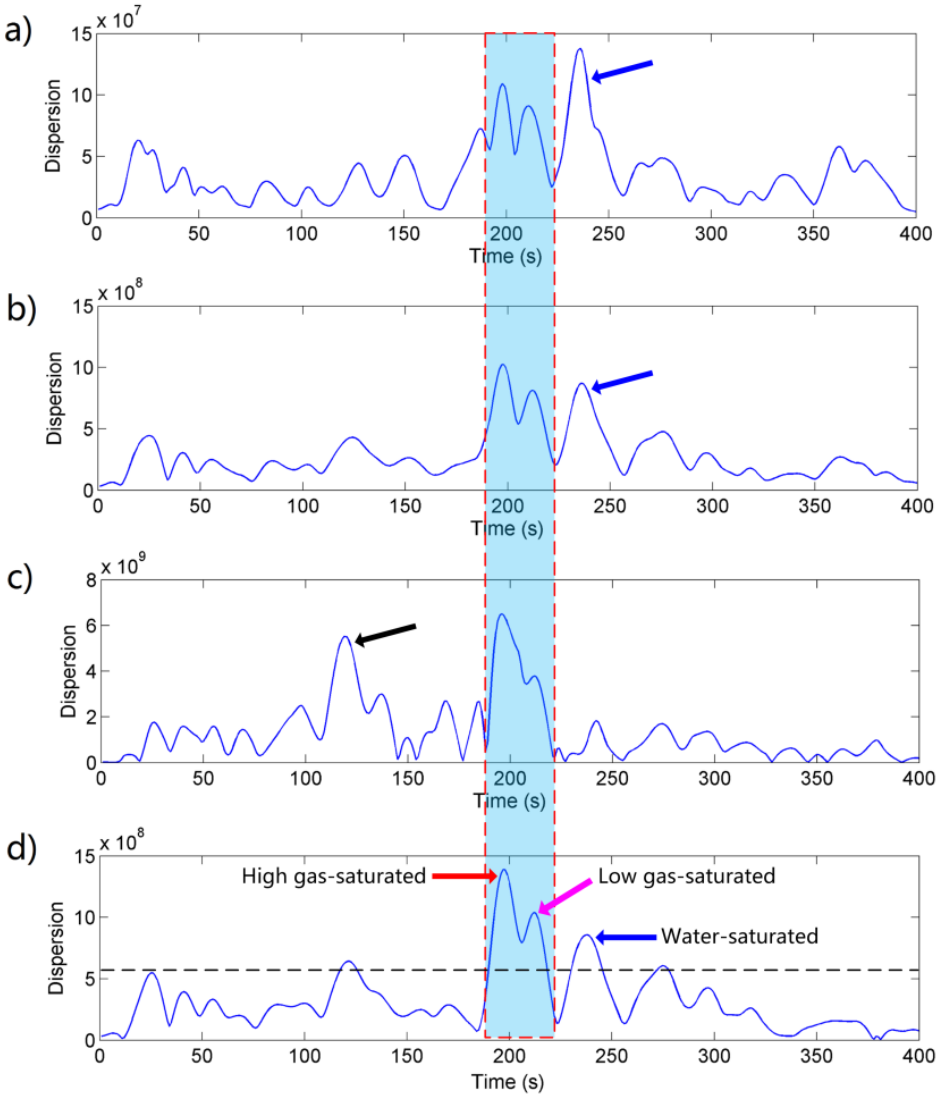

Fig. 11. Dispersion curves of (a) P-wave, (b) r = 4/3, (c) r = 3, and (d) our method selected at the location of well.

As shown in Fig. 11, all dispersion curves show significant dispersion anomalies in gas-saturated reservoirs (outlined by a cyan rectangle). However, the dispersion curves shown in Figs. 11a and 11b are greatly affected by the dispersion anomalies of water saturated (indicated by blue arrows). Both are disadvantage to the delineation for high gas saturation reservoir. The dispersion factor of r = 3 are greatly affected by the interference of top elastic layers (the black arrow shows), and it is difficult to identify the dispersion anomalies of the gas-saturated zone (Fig. 11c). The dispersion factor obtained by our method (Fig. 11d) only shows significant dispersion anomalies in the gas-saturated zone, whereas the background interference of elastic layers is very weak. Meanwhile, there are differences in dispersion degree when gas reservoirs saturated with different gas saturations. It means that the dispersion factor obtained by our proposed optimizing schemes has a much better capability for hydrocarbon detection and degraded the elastic characteristics.

Finally, we can calculate the dispersion results for seismic data volume by using the optimal parameters f_{opt} and r_{opt}. In Fig. 12, the dispersion profile of P-wave is compared with the dispersion profile obtained by our method. Note that the P-wave dispersion obtained by conventional FDAI method is failed to discriminate the reservoirs saturated with different gas saturation. However, the dispersion profile obtained by our method can exhibit the location and spatial distribution of the hydrocarbon reservoir with high gas-saturation and is less affected by the background interference. The dispersion slice extracted along the target layer (Fig. 13b) clearly delineates the spatial distribution and evident edge of the high gas-saturation reservoir. The gas reservoir correlates quite well with the known production. So the dispersion factor calculated by our method is the most sensitive to the fluids and can manifest the distinct dispersion anomalies of the hydrocarbon reservoirs with different gas saturations and degrade the background interference of elastic layers to the most extent.

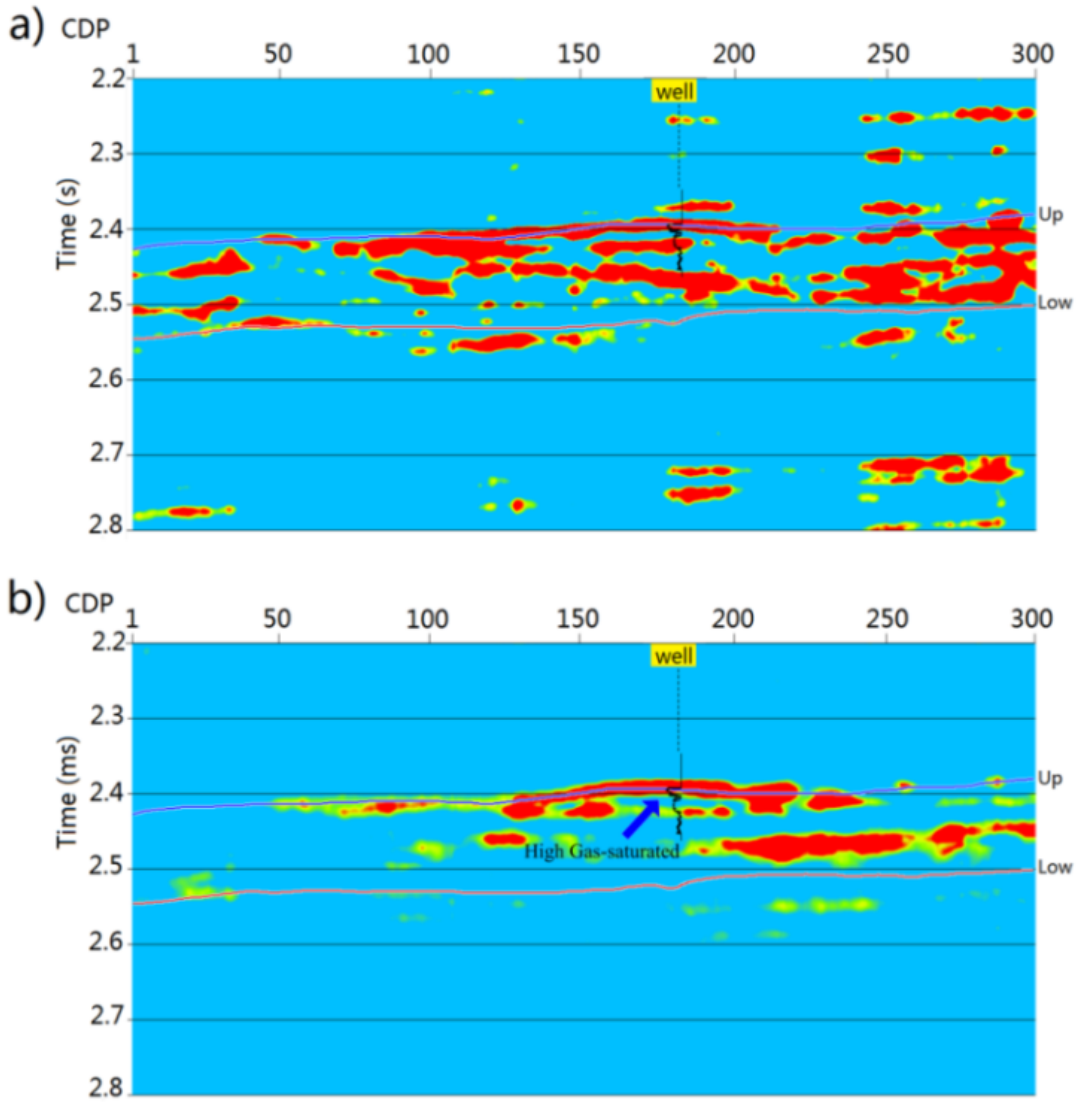

Fig. 12. The dispersion factor profile of (a) P-wave and (b) our method.

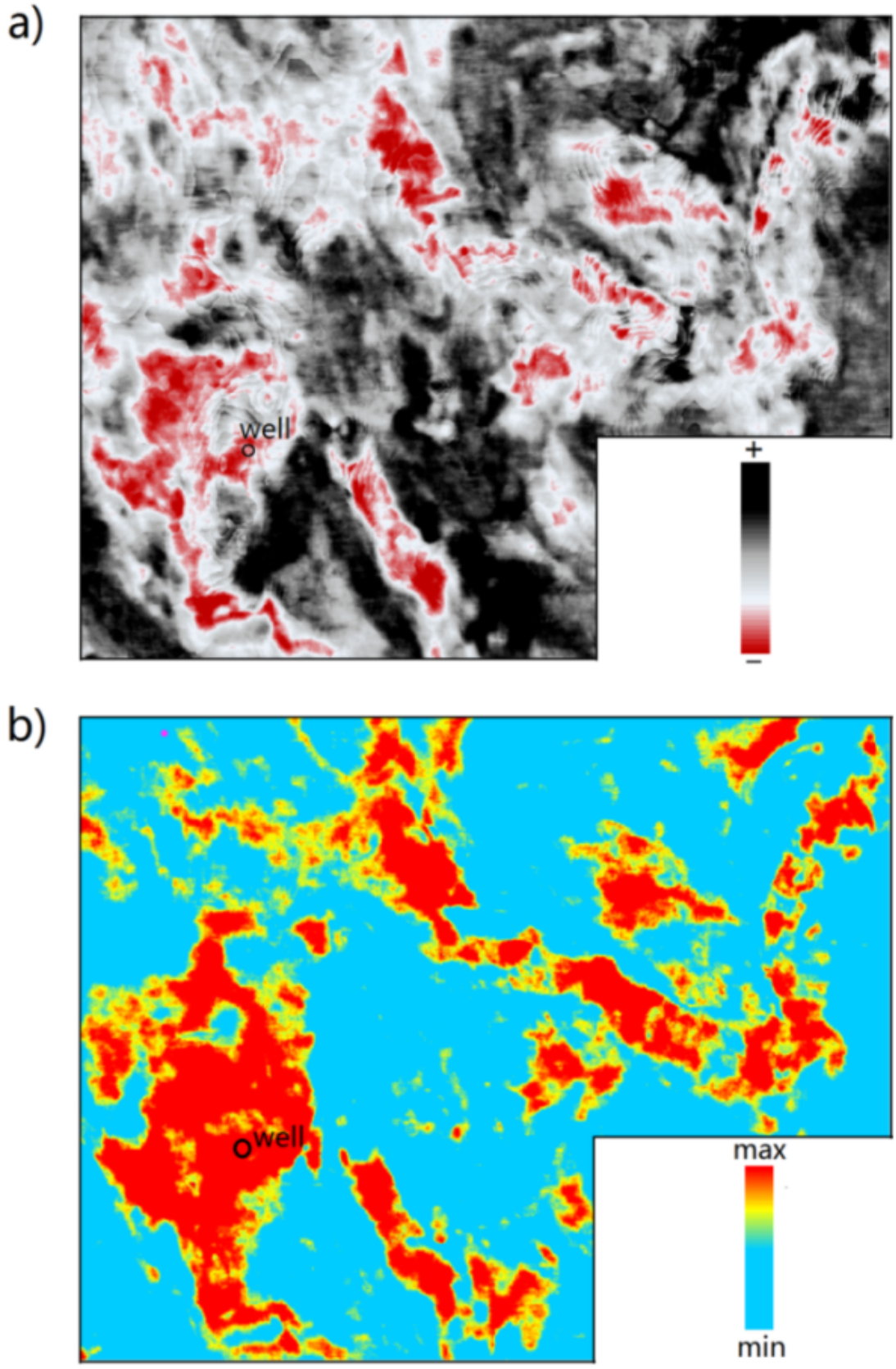

Fig. 13. (a) Seismic amplitude slice extracted through the reservoir with high gas saturation in the target interval and (b) its corresponding dispersion factor slice calculated by our method.

DISCUSSION AND CONCLUSION

The velocity dispersion and attenuation occur when the seismic wave travels through the fluid-saturated reservoirs and wave-induced fluid flow results in frequency-dependent reflection coefficients and AVO response. This helps to use the dispersion anomalies to detect the fluid-saturated reservoirs. The dispersion factor inferred from FDAI method is a significant indicator for fluid identification. In this paper, we proposed an optimal scheme of FDAI for selecting the most sensitive dispersion-related fluid factors to quantitatively delineate the reservoirs with high gas saturation.

The field data tests prove the effectiveness of the optimizing schemes. The dispersion factor inverted by the optimal reference frequency f_{opt} can maximize the dispersion anomalies of fluid-saturated reservoirs. Moreover, the optimal dispersion factor I_f selected by fluid indication coefficient can indicate the gas reservoir more accurately while it is less affected by the background interference of elastic layers. The results show that our optimal schemes of FDAI can provide the optimal dispersion factor to detect the location and spatial distribution of gas reservoirs with high gas saturation more accurately.

In order to get the more reliable and precise dispersion factor to delineate the hydrocarbon-bearing reservoir, there are also other key details should be taken into account in FDAI. First, the choice of reference elastic layer is of critical importance to spectral balancing operation and directly affects the accuracy of final inversion results. Second, in the real calculation, we should make full use of logging data to constrain the selection of reference frequency and elastic layer. In addition, the tuning effect can affect the frequency and amplitude features of seismic waves. The contributions of this phenomenon on FDAI will also directly affect the inversion results, which should not be ignored. Therefore，we need to consider the influence of various factors on the inversion results, and then select the optimal dispersion factor by comprehensive analysis to improve the accuracy of reservoir delineation.

ACKNOWLEDGEMENTS

This work was supported by the National Natural Science Foundation of China (Grant Nos. 41574130, 41874143 and 41374134), the National Science and Technology Major Project of China (Grant No. 2016ZX05014-001-009), the Sichuan Provincial Youth Science & Technology Innovative Research Group Fund (Grant No. 2016TD0023). We greatly thank the anonymous reviewer for the constructive comments and editorial suggestions that significantly improved the quality of the manuscript.

REFERENCES

Batzle, M., Han, D.H. and Hofmann, R., 2006. Fluid mobility and frequency-dependent seismic velocity-Direct measurements. Geophysics, 70(1): N1-N9.

Batzle, M. and Wang, Z., 1992. Seismic properties of pore fluids. Geophysics, 57: 1396-1408.

Beckwith, J., Clark, R. and Hodgson, L., 2017. Estimating frequency-dependent attenuation quality factor values from prestack surface seismic data. Geophysics, 82(1): O11-O22.

Biot, M.A., 1962. Mechanics of deformation and acoustic propagation in porous media. J. Appl. Phys., 33: 1482-1498.

Bradford, J.H., 2007. Frequency-dependent attenuation analysis of ground-penetrating radar data. Geophysics, 72(3): J7-J16.

Brown, R.L., 2009. Anomalous dispersion due to hydrocarbons: the secret of reservoir geophysics? The Leading Edge, 20: 168-171.

Carcione, J.M. and Picotti, S., 2006. P-wave seismic attenuation by slow-wave diffusion: effects of inhomogeneous rock properties. Geophysics, 71(3): O1-O8.

Castagna, J.P., Swan, H.W. and Foster, J.D., 1998. Framework for AVO gradient and intercept interpretation. Geophysics, 63: 948-56.

Chapman, M., Liu, E. and Li, X.Y., 2005. The influence of abnormally high reservoir attenuation on the AVO signature. The Leading Edge, 24: 1120-1125.

Chapman, M., Liu, E. and Li, X.Y., 2006. The influence of fluid sensitive dispersion and attenuation on AVO analysis. Geophys. J. Internat., 167: 89-105.

Chapman, M., Maultzsch, S., Liu, E. and Li, X.Y., 2003. The effect of fluid saturation in an anisotropic multi-scale equant porosity model. J. Appl. Geophys., 54: 191-202.

Chapman, M., Zatsepin, S.V. and Crampin, S., 2002. Derivation of a microstructural poroelastic model. Geophys. J. Internat., 151: 427-451.

Chen, S.Q., Li, X.Y. and Wang, S.X., 2012. The analysis of frequency-dependent characteristics for fluid detection: a physical model experiment. Appl. Geophys., 9: 195-206.

Chen, S.Q., Li, X.Y. and Wu, X.Y., 2014. Application of frequency-dependent AVO inversion to hydrocarbon detection. J. Seismic Explor., 23: 241-264.

Chen, X.H., He, Z.H. and Huang, D.J., 2008. Generalized S-transform and its time-frequency filtering. Signal Process., 24: 28-31.

Chen, X.H., He, Z.H., Pei, X.G., Zhong, W.L. and Yang, W., 2013. Numerical simulation of frequency-dependent seismic response and gas reservoir delineation in turbidites: A case study from China. J. Appl. Geophys., 94: 22-30.

Chen, X.H., Zhong, W.L., He, Z.H. and Zou, W., 2016. Frequency-dependent attenuation of compressional wave and seismic effects in porous reservoirs saturated with multi-phase fluids. J. Petrol. Sci. Engineer., 147: 371-380.

Chen, X.H., Zhong, W.L., Gao, G., Zou, W. and He, Z.H., 2017. Numerical analysis of Velocity dispersion in multi-phase fluid-saturated porous rocks. Pure Appl. Geophys., 174: 1219-1235.

Cheng, B.J., Xu, T.J. and Li, S.G., 2012. Research and application of frequency dependent AVO analysis for gas recognition. Chin. J. Geophys., 55: 608-613.

Dupuy, B. and Stovas, A., 2014. Influence of frequency and saturation on AVO attributes for patchy saturated rocks. Geophysics, 79(1): B19-B36.

Dvorkin, J., Mavko, G. and Nur, A., 1995. Squirt flow in fully saturated rocks. Geophysics, 60: 97-107.

Gary, D., 2002. Elastic inversion for Lame parameters. Expanded Abstr., 72nd Ann. Internat. SEG Mtg., Salt Lake city: 213-216.

Gazdag, B. and Sguazzero, P., 1984. Migration of seismic data by phase-shift plus interpolation. Geophysics, 49: 124-131.

Ghosal, D. and Juhlin, C., 2018. Estimation of dispersion attributes at seismic frequency - a case study from the Frigg-Delta reservoir, North Sea. J. Geophys. Engineer., 15: 1799-1810.

Gurevich, B., Makarynska, D., Paula, O.B. and Pervukhina, M., 2010. A simple model for squirt-flow dispersion and attenuation in fluid-saturated granular rocks. Geophysics, 75(6): N109-N120

Johnson, D.L., 2001. Theory of frequency-dependent acoustics in patch saturated porous media. J. Acoust. Soc. Am., 110: 682-694.

Korneev, V.A., Goloshubin, G.M., Daley, T.M. and Silin, D.M., 2004. Seismic low frequency effects in monitoring fluid-saturated reservoirs. Geophysics, 69: 522-532.

Liu, L.F., Cao, S.Y. and Wang, L., 2011. Poroelastic analysis of frequency-dependent amplitude-versus-offset variations. Geophysics, 76(3): C31-C40.

Mavko, G., Mukerji, T. and Dvorkin, J., 2009. The Rock Physics Handbook, 2nd ed. Cambridge University Press, Cambridge.

Müller, T. M., Gurevich, B. and Lebedev, M., 2010. Seismic wave attenuation and dispersion resulting from wave-induced flow in porous rocks - a review. Geophysics, 75(5): A147-A164.

de Paula, O., Pervukhina, M., Makarynska, D. and Gurevich, B., 2012. Modeling squirt dispersion and attenuation in fluid-saturated rocks using pressure dependency of dry ultrasonic velocities. Geophysics, 77(3): WA157-WA168.

Pride, S.R. and Berryman, J.G., 2003a. Linear dynamics of double-porosity dual permeability materials: Part 1 - Governing equations and acoustic attenuation. Phys. Rev. E, 68: 036603.

Pride, S.R. and Berryman, J. G., 2003b. Linear dynamics of double-porosity dual permeability materials: Part 2 - Fluid transport equations. Phys. Rev. E, 68: 036604

Quintal, B., 2012. Frequency-dependent attenuation as a potential indicator of oil saturation. J. Appl. Geophys., 82: 119-128.

Rubino, J.G. and Holliger, K., 2012. Seismic attenuation and velocity dispersion in heterogeneous partially saturated porous rocks. Geophys. J. Internat., 188: 1088-1102.

Russell, B. H., Hedlin, K. and Hilterman, F. J., 2003. Fluid-property discrimination with AVO: a Biot-Gassmann perspective. Geophysics, 68: 29-39.

Russell, B.H., Gray, D. and Hampson, D.P., 2011. Linearized AVO and poroelasticity. Geophysics, 76(3): C19-C29.

Silin, D.B. and Goloshubin, G., 2010. An asymptotic model of seismic reflection from a permeable layer. Transp. Porous Media, 83: 233-256.

Silin, D.B., Korneev, V.M., Goloshubin, G.M. and Patzek, T.W., 2006. Low-frequency asymptotic analysis of seismic reflection from a fluid-saturated medium. Transp. Porous Media, 62: 283-305.

Smith, G. C. and Gidlow, P. M., 1987. Weighted stacking for rock property estimation and detection of gas. Geophys. Prosp., 35: 993-1014.

White, J.E., 1975. Computed seismic speeds and attenuation in rocks with partial gas saturation. Geophysics, 40: 224-232.

Wiggins, R., Kenny, G.S. and McClure, C.D., 1983. A method for determining and displaying the shear wave reflectivities of a geologic formation. Europ. Patent Applicat.: 0113944.

Wilson, A., Chapman, M. and Li, X.Y., 2009. Frequency-dependent AVO inversion. Expanded Abstr., 79th Ann. Internat. SEG Mtg., Houston, 28: 341-345.

Wu, X.Y., Chapman, M. and Li, X.Y., 2012. Frequency-dependent AVO attribute: Theory and example. First break, 30: 67-72.

Wu, X.Y., Chapman, M., Li, X.Y. and Boston, P., 2014. Quantitative gas saturation estimation by frequency-dependent amplitude versus-offset analysis. Geophys. Prosp., 62: 1224-1237.

Xu, D., Wang, Y.H., Gan, Q.G. and Tang, J.M., 2011. Frequency-dependent seismic reflection coefficient for discriminating gas reservoirs. J. Geophys. Engineer., 8: 508-513.

Yang, J.D. and Zhu, H.J., 2018. A time-domain complex-valued wave equation for modeling viscoacoustic wave propagation. Geophys. J. Internat., 215: 1064-1079.

Yang, J.D. and Zhu, H.J., 2018. Viscoacoustic reverse time migration using a time-domain complex-valued wave equation. Geophysics, 83(6): S505-S519.

Zhang, S.X, Yin, X.Y. and Zhang, G.Z., 2011. Dispersion-dependent attribute and application in hydrocarbon detection. J. Geophys. Engineer., 8: 498-507.

Zhang, Z., Yin, X.Y. and Hao, Q.Y., 2014. Frequency-dependent fluid identification method based on AVO inversion. Chin. J. Geophys., 57: 4171-4184.
Zhong, W.L., Chen, X.H., Luo, X., Jiang, W. and Yang, W., 2017. Amplitude non-sensitive stratal dispersion shadow for dim spot reservoir delineation. Acta Geol. Sin. (Engl. ed.), 91: 1513-1514.
Zong, Z.Y., Yin, X.Y. and Wu, G.C., 2016. Frequency dependent elastic impedance inversion for interstratified dispersive elastic parameters. J. Appl. Geophys., 131: 84-93.

APPENDIX A

FREQUENCY-DEPENDENT VELOCITY AND ATTENUATION

Chapman et al. (2003) proposed a local squirt-flow model for a multi-scale equant porosity model， which is based on a squirt flow mechanism in fractured porous rocks with the pore space consists of spherical pores, micro-cracks and an aligned set of fractures. The poroelastic model can be used to reproduce dispersion and attenuation results even in the low- and high-frequency limits, i,e., at any frequency (Chapman, 2003; Mavko et al., 2009). We then use the dynamic equivalent-medium theory to analyze the velocity dispersion and attenuation in multi-scale porosity fluid-saturated rocks. The element of the effective stiffness tensor C_{ijkl} can take the form

$$C_{ijkl} = C^0_{ijkl} - \phi_p C^1_{ijjkl} - \varepsilon_c C^2_{ijkl} - \varepsilon_f C^3_{ijkl} \quad , \tag{A-1}$$

where C^0 is the isotropic background elastic tensor of the stiffness matrix with the Lamé parameters λ and μ. The corrections C^1, C^2, and C^3 multiplied by the equant pores ϕ_p, microcrack density ε_c and fracture density ε_f, are functions of the Lamé parameters, fluid properties, fracture length, time scale parameter τ and frequency. The stiffness tensor elements C_{ijkl} are related to the contribution of the equant pores, the random microcracks and the aligned fractures, the stiffness tensor C_{ijkl} is

$$\begin{aligned} C^{iso}_{ijkl}(\omega) = {} & C^{iso}_{ijkl}(\Lambda, \mathrm{M}, \omega) - \phi_p C^1_{ijkl}\left(\lambda_0, \mu_0, \omega, \tau, \phi, k_f\right) \\ & - \varepsilon_c C^2_{ijkl}\left(\lambda_0, \mu_0, \omega, \tau, \phi, k_f\right) - \varepsilon_f C^3_{ijkl}\left(\lambda_0, \mu_0, \omega, \tau, \phi, k_f\right) \end{aligned} \tag{A-2}$$

where Λ and M are functions of the Lamé parameters λ^0 and μ^0 , which calculated by the velocities of the unfractured rock, v_p^0 and v_s^0, measured at the reference frequency f_0. The form given as

$$\begin{aligned} \Lambda &= \lambda_0 + \Phi_{c,p}\left(\lambda_0, \mu_0, \omega_0, \tau_0\right) \\ \mathrm{M} &= \mu_0 + \Phi_{c,p}\left(\lambda_0, \mu_0, \omega_0, \tau_0\right) \end{aligned} \quad , \tag{A-3}$$

where $\Phi_{c,p}$ refers to the corrections to the elastic tensor proportional to ε_c and ϕ_p.

We can calculate the frequency-dependent velocity and attenuation based on the five independent stiffness constants. The matrix representation of frequency-dependent elastic stiffness calculated from Chapman's (2003) model has the following form

$$\begin{bmatrix} C_{11} & C_{12} & C_{13} & 0 & 0 & 0 \\ C_{12} & C_{11} & C_{13} & 0 & 0 & 0 \\ C_{13} & C_{13} & C_{33} & 0 & 0 & 0 \\ 0 & 0 & 0 & C_{44} & 0 & 0 \\ 0 & 0 & 0 & 0 & C_{44} & 0 \\ 0 & 0 & 0 & 0 & 0 & C_{66} \end{bmatrix}, \quad C_{66} = \frac{1}{2}\left(C_{11} - C_{12}\right) \quad . \tag{A-4}$$

Then, we can obtain the corresponding frequency-dependent complex compressional and shear velocities $\tilde{v}_p(\omega)$ and $\tilde{v}_s(\omega)$

$$\begin{aligned} \tilde{v}_p(\omega) &= \left(C_{11}\sin^2\theta + C_{33}\cos^2\theta + C_{44} + \sqrt{M}\right)^{1/2}\left(2\rho\right)^{-1/2} \\ \tilde{v}_s(\omega) &= \left(C_{11}\sin^2\theta + C_{33}\cos^2\theta + C_{44} - \sqrt{M}\right)^{1/2}\left(2\rho\right)^{-1/2} \end{aligned} \tag{A-5}$$

where

$$M = \left[\left(C_{11} - C_{44}\right)\sin^2\theta - \left(C_{33} - C_{44}\right)\cos^2\theta\right]^2 + \left(C_{13} + C_{44}\right)^2 \sin^2 2\theta \quad . \tag{A-6}$$

Next, the frequency-dependent phase velocities and inverse quality factors are given by

$$v_p(\omega) = \frac{1}{\mathrm{Re}\left[1/\tilde{v}_p(\omega)\right]}, v_s(\omega) = \frac{1}{\mathrm{Re}\left[1/\tilde{v}_s(\omega)\right]} \tag{A-7}$$

$$\frac{1}{Q_p(\omega)} = \frac{\mathrm{Im}\left[\tilde{v}_p(\omega)^2\right]}{\mathrm{Re}\left[\tilde{v}_p(\omega)^2\right]}, \quad \frac{1}{Q_s(\omega)} = \frac{\mathrm{Im}\left[\tilde{v}_s(\omega)^2\right]}{\mathrm{Re}\left[\tilde{v}_s(\omega)^2\right]} \quad . \tag{A-8}$$

APPENDIX B

NUMERICAL SIMULATION OF SEISMIC RESPONSES

To illustrate the role of fluids on compressional seismic waves traveling through saturated reservoirs, we reduced the 2D scalar wave equation (Gazdag and Sguazzero, 1984) to the 1D edition to employ the simulation of wave propagation by phase-shift wavefield extrapolation in the frequency wavenumber (F-K) domain. The equation form of the 1D edition given by

$$\frac{\partial^2 u}{\partial t^2} - v^2 \frac{\partial^2 u}{\partial z^2} = 0 \quad , \tag{B-1}$$

where u is the displacement, z is the depth, t denotes the two-way travel time, and v is the phase velocity in m/s.

According to the frequency-dependent velocities, the frequency-dependent reflection coefficients versus incident angles can be calculated by the flowing linear approximation equation that was modified from Wiggins et al. (1983).

$$R_P(\omega,\theta) = A(\omega) + B(\omega)\sin^2\theta + C(\omega)\tan^2\theta\sin^2\theta \quad , \tag{B-2}$$

where

$$\begin{cases} A(\omega) = \frac{1}{2}\left[\frac{\Delta v_p(\omega)}{v_p(\omega)} + \frac{\Delta\rho}{\rho}\right], \\ B(\omega) = \frac{1}{2}\frac{\Delta v_p(\omega)}{v_p(\omega)} - 4\left[\frac{v_s(\omega)}{v_p(\omega)}\right]^2 \frac{\Delta v_s(\omega)}{v_s(\omega)} - 2\left[\frac{v_s(\omega)}{v_p(\omega)}\right]^2 \frac{\Delta\rho}{\rho}, \\ C(\omega) = \frac{1}{2}\frac{\Delta v_p(\omega)}{v_p(\omega)}. \end{cases} \tag{B-3}$$

For a harmonic wave given by:

$$u = e^{-ik_z z} e^{i\omega t} \quad . \tag{B-4}$$

Substituting eq. (B-4) into eq. (B-1), we have

$$\left(i\omega\right)^2 - v^2\left(ik_z\right)^2 = 0 \quad . \tag{B-5}$$

Then, we obtain the vertical wave number in the frequency domain related to the frequency-dependent complex velocity $v(\omega)$, and the relationship can be expressed as:

$$K_z\left(\omega\right) = \frac{\omega}{v\left(\omega\right)} \tag{B-6}$$

In the numerical simulation, the wave field extrapolation based on the phasIe-shift method of eq. (B-4) in the F-K domain, is expressed as:

$$u\left(z + \Delta z, \omega\right) = u\left(z, \omega\right) e^{ik_z(\omega)\Delta z} \tag{B-7}$$

Then we can obtain the frequency-dependent seismic response of a compressional wave from the models.